Mon. Not. R. Astron. Soc. **000**, 000–000 (0000) Printed 22 February 2005 (MN LATEX style file v2.2)

Spitzer Imaging of i'-drop Galaxies: Old Stars at $z \approx 6$

Laurence P. Eyles[1], Andrew J. Bunker[1], Elizabeth R. Stanway[2], Mark Lacy[3], Richard S. Ellis[4], Michelle Doherty[5]

[1] *School of Physics, University of Exeter, Stocker Road, Exeter, EX4 4QL, U.K.*
email: eyles@astro.ex.ac.uk
[2] *Astronomy Department, University of Wisconsin-Madison, 475 N. Charter Street, Madison, WI 53706, U.S.A.*
[3] *Spitzer Science Center,California Institute of Technology, Mail Code 220-6, 1200 E. California Blvd., Pasadena, CA 91125, U.S.A.*
[4] *California Institute of Technology, Mail Stop 169-327, Pasadena, CA 91109, U.S.A.*
[5] *Institute of Astronomy, Madingley Road, Cambridge, CB3 0HA, U.K.*

Submitted to MNRAS

ABSTRACT

We present new evidence for mature stellar populations with ages $> 100\,$Myr in massive galaxies ($M_{\rm stellar} > 10^{10}\,M_{\odot}$) seen at a time when the Universe was less than 1 Gyr old. We analyse the prominent detections of two $z \approx 6$ star-forming galaxies (SBM03#1 & #3) made at wavelengths corresponding to the rest-frame optical using the IRAC camera onboard the *Spitzer Space Telescope*. We had previously identified these galaxies in *HST*/ACS GOODS images of Chandra Deep Field South through the "i'-drop" Lyman break technique, and subsequently confirmed spectroscopically with the Keck telescope. The new *Spitzer* photometry reveals significant Balmer/4000 Å discontinuities, indicative of dominant stellar populations with ages $> 100\,$Myr. Fitting a range of population synthesis models to the *HST/Spitzer* photometry yields ages of $250 - 650\,$Myr and implied formation redshifts $z_f \approx 7.5 - 13.5$ in presently-accepted world models. Remarkably, our sources have best-fit stellar masses of $2 - 4 \times 10^{10}\,M_{\odot}$ (95% confidence) assuming a Salpeter initial mass function. This indicates that at least some galaxies with stellar masses $> 20\%$ of those of a present-day L^* galaxy had already assembled within the first Gyr after the Big Bang. We also deduce that the past average star formation rate must be comparable to the current observed rate ($\mathrm{SFR_{UV}} \sim 5 - 30\,M_{\odot}\,\mathrm{yr}^{-1}$), suggesting that there may have been more vigorous episodes of star formation in such systems at higher redshifts. Although a small sample, limited primarily by Spitzer's detection efficiency, our result lends support to the hypothesis advocated in our earlier analyses of the Ultra Deep Field and GOODS *HST*/ACS data. The declining global star formation density and presence of established systems at $z \approx 6$ suggests long-lived sources at earlier epochs ($z > 7$) played a key role in reionizing the Universe.

Key words:
galaxies: evolution – galaxies: formation – galaxies: starburst – galaxies: individual: SBM03#1, SBM03#3, GLARE#3001, GLARE#3011 – galaxies: high redshift – galaxies: stellar content

1 INTRODUCTION

In recent years, advances in detector efficiency, large ground-based telescopes and space-based observatories such as the *Hubble Space Telescope (HST)* and *Spitzer Space Telescope*, have revolutionized studies of the high redshift Universe. Searches based on Lyman-α emission are now at last uncovering many galaxies at $2 < z < 7$ (e.g., Kodaira et al. 2003; Rhoads et al. 2004). The Lyman-break technique (Steidel, Pettini & Hamilton 1995; Steidel et al. 1996; 1999) has likewise proved successful in selecting high-redshift star-forming galaxies. This utilises the rest-UV continuum break seen shortward of Lyman-α and caused by H I absorption in the intergalactic medium.

The redshift range $z \approx 6$ is of great importance, as it heralds the end of the reionization of the Universe (Becker et al. 2001; Kogut et al. 2003) which might be achieved through star formation. Using *HST* and the new Advanced Camera for Surveys (ACS; Ford et al. 2003), the Lyman-break technique has been pushed to this early epoch (Stan-

way, Bunker & McMahon 2003; Bouwens et al. 2004; Yan & Windhorst 2004; Giavalisco et al. 2004) by using the i' and z' filters to isolate i'-drop galaxies. Ground-based follow-up spectroscopy (Bunker et al. 2003; Stanway et al. 2004a,b; Dickinson et al. 2004) has shown that a colour cut of $(i'-z')_{AB} > 1.5$ mag reliably finds star-forming galaxies at $z \approx 6$ with modest foreground contamination (primarily from low-mass stars, and passively evolving galaxies at $z \sim 1-2$).

Yet a key part of the puzzle is missing: the i'-band drops are selected in the rest-frame UV, and are therefore known to be actively forming stars. However, it is unclear whether these objects suffer from significant reddening due to dust (in which case the star formation rates will have been underestimated), or if there is an underlying older stellar population which has been recently rejuvenated. Deep publicly-available *Spitzer* imaging with the Infrared Array Camera (IRAC; Fazio et al. 2004) as part of the Great Observatories Origins Deep Survey[1] (GOODS; Dickinson & Giavalisco 2003; Dickinson et al. *in prep*) allows us to address both questions.

A key benefit of Spitzer photometry arises because the IRAC camera samples wavelengths longwards of the age-sensitive Balmer & 4000Å breaks at $z \approx 6$. Accordingly, we have analysed the IRAC images of GOODS-South field (centred on the *Chandra* Deep Field South, Giacconi et al. 2002), where we have already selected i'-drop galaxies from the GOODS-S ACS images (Stanway, Bunker & McMahon 2003) and the Ultra-Deep Field (UDF; Bunker et al. 2004).

Our goal in this paper is thus to focus on the infrared properties of four $z \approx 6$ galaxies for which there are robust spectroscopic redshifts, based on Lyman-α emission. The properties of the entire i'-drop population in the GOODS fields is considered in a forthcoming paper (Eyles et al. *in prep*). Our four confirmed sources include two sources from Stanway, Bunker & McMahon (2003): the brightest confirmed i'-drop in the GOODS-S field (with $z' = 24.7$ mag) SBM03#3 (with a spectroscopic redshift of $z = 5.78$ from Keck/DEIMOS, Bunker et al. 2003); and the brightest i'-drop in the UDF, SBM03#1 with $z' = 25.3$ mag (spectroscopically confirmed with Keck/DEIMOS by Stanway et al. 2004a). Both of these spectroscopic redshifts were independently confirmed by Dickinson et al. (2004). The other two sources come from the Gemini Lyman-α at Reionization Era (GLARE, Stanway et al. 2004b) spectroscopy with Gemini/GMOS: GLARE#3001 ($z = 5.79$, $z' = 26.4$ mag) and GLARE#3011 ($z = 5.94$, $z' = 27.2$ mag).

A plan of the paper follows. In Section 2 we describe the *Spitzer* imaging data and the methods used to fit stellar populations to the broad band photometry derived collectively from *Spitzer*, *HST* ACS & NICMOS images, and ground-based near-IR data. We discuss the implications of the age and our stellar mass estimates in Section 3. Our conclusions are presented in Section 4. Throughout we adopt the standard "concordance" cosmology of $\Omega_M = 0.3$, $\Omega_\Lambda = 0.7$, and use $H_0 = 70\,\mathrm{km\,s^{-1}\,Mpc^{-1}}$. All magnitudes are on the *AB* system (Oke & Gunn 1983).

[1] see `http://www.stsci.edu/ftp/science/goods/`

2 OBSERVATIONS, DATA REDUCTION AND STELLAR POPULATION FITTING

2.1 *Spitzer* Observations

We concentrate here on the shortest-wavelength *Spitzer* images of GOODS-S taken with IRAC as part of the "Super Deep" Legacy programme (PID 194, Dickinson et al. *in prep*). We have analysed the first half of the GOODS-S *Spitzer* data, taken with 39 Astronomical Observation Requests (AORs) observed between 8–16 February 2004.

The IRAC camera comprises four channels, each with a 256^2 InSb array imaging a $5.2' \times 5.2'$ field with a pixel size of $\approx 1\farcs22$. Images were taken through four broad-band infrared filters, with central wavelengths at approximately $\lambda_{\rm cent} = 3.6\,\mu$m, $4.5\,\mu$m, $5.6\,\mu$m and $8.0\,\mu$m (channels 1–4), and widths of $\Delta\lambda_{\rm FWHM} = 0.68, 0.87, 1.25, 2.53\,\mu$m respectively. The individual frame times for each channel were 200 s (except those taken at $8.0\,\mu$m, which comprise 4 integrations of 50 s at each position). Over the course of the 39 AORs, a large 2×2 mosaic of pointings was executed, with smaller random sub-dithers when the pattern was repeated, giving a $10' \times 10'$ coverage for each filter. Each AOR comprised 10–11 pointings. Channels 1 & 3 ($3.6\,\mu$m & $5.6\,\mu$m) have the same pointing, offset by $6.7'$ from the common pointing of channels 2 & 4 ($4.5\,\mu$m & $8.0\,\mu$m). As a result, only a portion of the field is observed in all four wavebands. Once data from the second epoch (when the telescope has rotated by 180 degrees) has been gathered, images of the entire $10' \times 16.5'$ field matching the GOODS-S ACS survey (Giavalisco 2003) in all four filters will be available. Meanwhile, by design, the overlap region common to all filters covers the Ultra Deep Field (Beckwith et al. 2003). The total exposure time in each channel is ≈ 86 ksec, depending on location.

2.2 Data Reduction

For our investigation, we used the pipeline-processed IRAC images[2] at the 'Post-Basic Calibrated Data' (PBCD) stage, details of which can be found in the Infrared Array Camera Data Handbook, Version 1.0 (Reach et al. 2004). The main steps in the pipeline include dark current subtraction, application of flatfields, flux calibration (in units of MJy/sr) and mosaicing of the individual frames of each AOR after application of a distortion correction. PBCD sets have a refined pointing solution to an accuracy of $0\farcs2$ derived from 2MASS point source catalogue objects in the field of view. Outlier rejection is performed during the mosaicing process.

We used IRAF to combine the 39 PBCD mosaics (one for each AOR), which were taken at different telescope roll angles. The IRAF task `wregister` was used to rotate the frames to a common roll angle, then the 39 frames were combined using `imcombine`, during which residual unrejected cosmic rays, bad pixels, and the column pull-down and muxbleed detector effects were removed using a percentile clipping method. The PBCD images were converted from units of surface brightness (MJy/sr) into flux units of μJy per pixel by multiplying the data units by $10^{12}\times$ (pixel solid

[2] The PBCD images are available from `http://ssc.spitzer.caltech.edu/popular/goods/irac_04/`

angle): a numerical factor of 34.98. The images were matched to the v1.0 reduced z'-band tiles of the GOODS-S field released by the GOODS team[3]. The astrometry was found to be consistent to within ≈ 0.2 IRAC pixels ($\approx 0\farcs3$).[4]

In the final coadded images, we measured the FWHM of the PSF to be $\approx 1\farcs5$ in channels 1 & 2 (3.6 & 4.5 μm), and $\approx 1\farcs8$ in channel 3 (5.6 μm) & $\approx 2\farcs1$ in channel 4 (8 μm). Even for the short-wavelength IRAC images, the *Spitzer* PSF is much larger than the typical size of the $z \approx 6$ i'-band drop galaxies (whose half-light radii $r_{hl} < 0\farcs2$, Bunker et al. 2004). At *Spitzer* resolution, these galaxies are clearly unresolved and so we treat them as point sources.

To construct spectral energy distributions of our 4 spectroscopically-confirmed i'-band drop galaxies in the GOODS-S field (detailed in Section 1 and Table 1) we undertook aperture photometry in the various images. In order to maximize the signal-to-noise ratio (S/N) and minimize possible confusion with other foreground objects, we used a diameter $\approx 1.5 \times$ FWHM, appropriate for unresolved objects. The aperture diameters were 2, 2, 2.5 & 3 IRAC pixels for the 4 channels (3.6, 4.5, 5.6 & 8.0 μm), corresponding to $2\farcs4$, $2\farcs4$, $3\farcs0$, & $3\farcs7$. We used the IRAF `digiphot.phot` package to measure the enclosed flux at the exact coordinates determined from the GOODSv1.0 and UDF z'-band images, taking the residual background from an annulus between $12''$ and $24''$ radius. We applied aperture corrections to compensate for the flux falling outside the aperture: these were ≈ 0.7 mag, as determined from bright, but unsaturated point sources in the images. These aperture corrections are consistent with those derived for the First Look Survey (Lacy et al. 2005).

Checks were made to ensure the objects were not contaminated by the presence of any neighbouring bright foreground sources. An object was deemed to be uncontaminated if no bright source lay within a $4''$ radius from it. All four objects satisfied this criteria; the bright source close to SBM03#3 lies on the $4''$ limit (Figure 2). The *Spitzer* magnitudes in Table 2 have the neighbour subtracted out (i.e., are deblended) but this has only a $\approx 5\%$ effect on the measured flux in our $2\farcs4$-diameter aperture; less than the error bar.

The noise for each of the four channels was checked in two different ways. First, we derived an estimate based on a Poisson model using the detector gain, number of frames combined, and the background counts (adding back the zodiacal background estimate subtracted by the pipeline but recorded in the header). Secondly, we measured the standard deviation in background counts of the images. As the mosaicing process introduces correlations between pixels, we also made noise estimates using the individual BCDs and assuming it decreased as the square root of the number of frames. These estimates lead to 3σ limiting AB magnitudes of 26.5 and 26.1 in $2\farcs4$ apertures in channels 1 and 2, respectively, and 23.8 and 23.5 in $3\farcs0$ apertures in channels 3 and 4, respectively. There will be additional background fluctuations caused by faint galaxies (i.e. confusion noise), which will increase the noise. Both methods produce consistent estimates.

Table 2 lists the measured AB magnitudes (corrected to approximate total magnitudes through an aperture correction) for the IRAC 3.6 μm, 4.5 μm and 5.6 μm channels. None of the sources were detected at $> 3\,\sigma$ in the 5.6 & 8 μm channels, although SBM03#3 has a very marginal ($2\,\sigma$) detection at 5.6 μm ($AB = 24.4 \pm 0.7$). In the short-wavelength channels, SBM03#1 & #3 are well-detected ($> 10\,\sigma$, $AB \approx 24$), and we have a more marginal $3\,\sigma$ detection of GLARE#3001 ($z'_{AB} = 26.4$) at $AB \approx 26$. Only SBM03#1 is detected at 4.5 μm – SBM03#3 falls outside the region surveyed so far in this filter, and GLARE#3001 is undetected. The fainter GLARE#3011 ($z'_{AB} = 27.2$) was undetected at all IRAC wavelengths. For the *HST* photometry, we use the ACS i'-band and z'-band magnitudes from Stanway, Bunker & McMahon (2003) from GOODS-S and, in the case of SBM03#1, from the deeper UDF (Bunker et al. 2004). These magnitudes are also corrected to a total flux through an aperture correction. We use NICMOS magnitudes (Thompson et al. *in prep*) in F110W and F160W ('J' and 'H' band) from Stanway, McMahon & Bunker (2005) for SBM03#1, and for the others we used v1.0 of the ESO VLT/ISAAC GOODS/EIS images[5] in the J and K_s bands (Vandame et al. *in prep*). In the ground-based near-infrared ISAAC images, we used $1''$-diameter apertures. The seeing varied across the ISAAC field, as different tiles were taken over many nights, so we determined the aperture correction from unresolved sources in each tile. For the J- and K_s-band images the seeing is typically good (FWHM $= 0\farcs4 - 0\farcs5$), and the aperture correction is $\approx 0.3 - 0.5$ mag.

The galaxy SBM03#3 is towards the edge of the released ESO/VLT imaging, where fewer frames overlap and the noise is higher. Its K_s magnitude seems to be anomalously faint (a $3\,\sigma$ detection at $K_{AB} = 25.5$, twice as faint as the shorter-wavelength z' and J, which have $AB = 24.7$ mag, and four times fainter than the longer-wavelength IRAC 3.6 μm detection at $AB = 24.0$). We still include the K_s filter in the fitting of the stellar populations (Section 2.3), but caution that the K_s magnitude may not be reliable. Fortunately, this filter makes minimal difference to the best-fit populations as its statistical weighting is low.

2.3 Spectral Energy Distributions

The final step in the reduction process is the construction of spectral energy distributions (SEDs) for the chosen sources. In order to compare our photometry with stellar spectral synthesis models, we utilise the latest Bruzual & Charlot (2003, hereafter B&C) isochrone synthesis code. We use the Padova 1994 evolutionary tracks (preferred by B&C 2003). The models utilise 221 age steps from 10^5 to 2×10^{10} yr, approximately logarithmically spaced. Models with Salpeter (1955) initial mass functions (IMF) were selected, although

[3] Available from `ftp://archive.stsci.edu/pub/hlsp/goods/v1`

[4] While our reduction was underway, the GOODS team released an enhanced dataset, employing a 'multidrizzle' technique similar to that used successfully on *HST*/ACS GOODS data. This provides combined images with a pixel scale of $\approx 0\farcs6$. These were used to provide a consistency check for the further reduction we conducted using IRAF. Upon cross-checking the astrometry, photometry and noise properties, they were found to be consistent to 0.1 mag and $0\farcs3$.

[5] Available from `http://www.eso.org/science/goods/releases/20040430/`

ID	RA	Dec	redshift
SBM03#1†	03:32:40.01	-27:48:15.0	5.83
SBM03#3	03:32:25.61	-27:55:48.7	5.78
GLARE#3001	03:32:46.04	-27:49:29.7	5.79
GLARE#3011	03:32:43.10	-27:45:17.6	5.94

† this is also known as GLARE#1042 (Stanway et al. 2004b), #20104 (Bunker et al. 2004), SiD002 (Dickinson et al. 2004) and YW01a (Yan & Windhorst 2004).

Table 1. The four spectroscopically-confirmed i'-drop galaxies in the GOODS-South Field.

in Section 3.5 we also consider the effect of adopting a Chabrier (2003) IMF. There are 6900 wavelength steps, with high resolution (FWHM 3 Å) and 1 Å pixels over the wavelength range of 3300 Å to 9500 Å (unevenly spaced outside this range). From the full range of metallicities offered by the code, we considered both solar and 1/5th solar models. From several star formation histories available, a single stellar population (SSP – an instantaneous burst), a constant star formation rate (SFR), and exponentially decaying (τ) SFR models were used.

For each of the four i'-drops with spectroscopic redshifts, the filters were corrected to their rest-frame wavelengths by the appropriate redshift factor. The measured flux at each waveband was averaged over the filter transmission profiles, and the best-fit age model was computed by minimising the reduced χ^2, using the measured errors on the magnitudes. The Bruzual & Charlot spectra are normalized to an initial mass of $1\,M_{\odot}$ for the instantaneous burst SSP model, and an SFR of $1\,M_{\odot}\,\mathrm{yr}^{-1}$ for the continuous star formation model. The fitting routine returned the normalisation for the model which was the best-fit to the broad band photometry (i.e., minimized the reduced χ^2) – this normalisation was then used to calculate the corresponding best-fit stellar mass (see Section 3.3).

Although some of our data points (particularly from the *HST*/ACS imaging) have $S/N > 10$, we set the minimum magnitude error to be $\Delta(\mathrm{mag}) > 0.1$ to account for calibration uncertainties. During this process, the i'-band flux was ignored, as this band is prone to contamination due to Lyman-α forest absorption shortwards of Lyman-α ($\lambda_{\mathrm{rest}} = 1216$ Å) and also emission line contamination due to Lyman-α itself.

3 ANALYSIS

For two of the spectroscopically-confirmed galaxies (SBM03#1 & #3) we have robust *Spitzer* detections at $3.6\,\mu$m of $AB \approx 24$ mag ($> 10\,\sigma$), with the fainter GLARE sources marginally detected (GLARE#3001) or undetected (GLARE#3011). Progressing in increasing wavelength from the *HST*/ACS z'-band and near-infrared ($0.9 - 2.2\,\mu$m) to the *Spitzer*/IRAC $3.6\,\mu$m channel, the two well-detected i'-drops brighten by $\Delta(\mathrm{mag})_{AB} = 0.8$ (Figures 4 & 5) – a factor of 2 in flux density, f_{ν}. SBM03#1 is also robustly detected with a similar magnitude at $4.5\,\mu$m. We now consider the implications of the spectral energy distributions of these i'-drops, specifically which star formation histories can produce the observed spectral breaks between $2.2 - 3.6\,\mu$m.

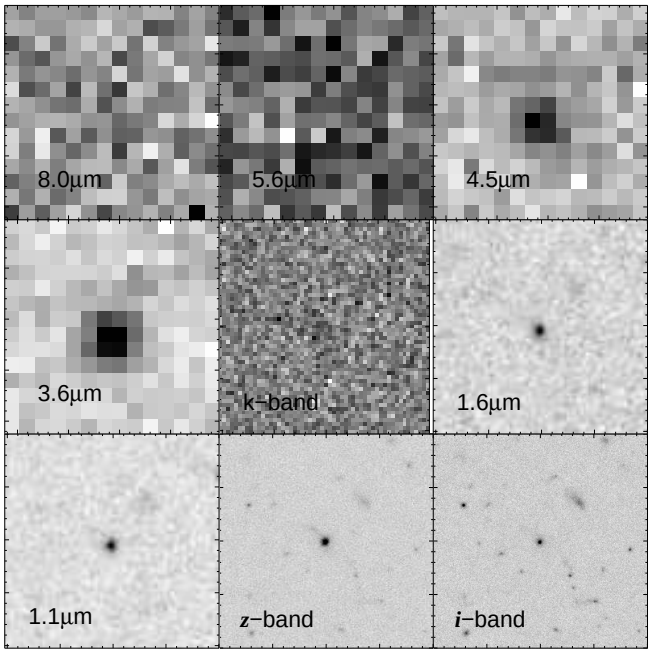

Figure 1. Images of SBM03#1 ($z = 5.83$), taken with *HST*/ACS (i'- and z'-band); *HST*/NICMOS (F110W 'J-band' and F160W 'H-band'), VLT/ISAAC K_s-band and the 4 *Spitzer* channels (3.6–8.0 μm). Each panel is 8 arcsec across (a projected distance of 50 kpc).

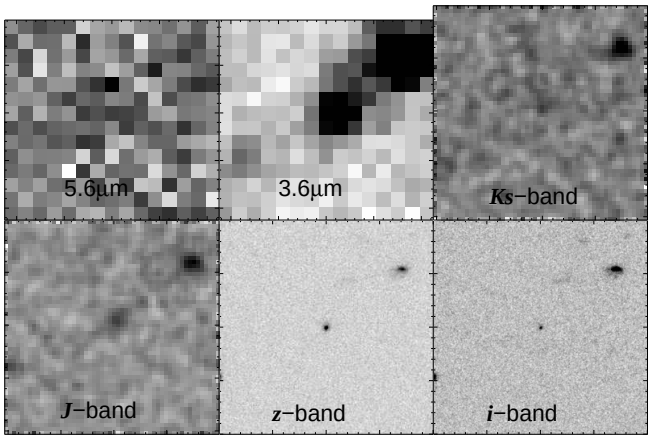

Figure 2. Images of SBM03#3 ($z = 5.78$), taken with *HST*/ACS (i'- and z'-band); VLT/ISAAC J- and K_s-bands and *Spitzer* channels 3.6 & 5.6 μm. Each panel is 8 arcsec across (a projected distance of 50 kpc). The J and K_s band images have been smoothed using a 3-pixel box.

ID	i'	z'	J	K_s	3.6 μm	4.5 μm	5.6 μm
SBM03#1	26.99 ± 0.03	25.35 ± 0.02	$25.54^{\dagger} \pm 0.04$	25.14 ± 0.22	24.24 ± 0.09	24.42 ± 0.15	> 23.8 ($3\,\sigma$)
SBM03#3	26.27 ± 0.13	24.67 ± 0.03	24.72 ± 0.15	$25.55 \pm 0.40^{\diamond}$	23.94 ± 0.07	—	24.39 ± 0.69
GLARE#3001	28.03 ± 0.14	26.37 ± 0.06	26.11 ± 0.32	25.22 ± 0.32	25.88 ± 0.36	> 26.1 ($3\,\sigma$)	> 23.8 ($3\,\sigma$)
GLARE#3011	> 28.8 ($3\,\sigma$)	27.15 ± 0.12	> 26.2 ($3\,\sigma$)	26.60 ± 0.94	> 26.5 ($3\,\sigma$)	> 26.1 ($3\,\sigma$)	> 23.8 ($3\,\sigma$)

$^{\diamond}$ The K_s magnitude of SBM03#3 is anomalously faint.

† From NICMOS F110W imaging (Stanway, McMahon & Bunker 2004); the F160W magnitude is $H_{AB} = 25.51 \pm 0.05$

Table 2. Magnitudes (AB system) of four i'-band drop galaxies. SBM03#3 is not in the field of view for the 4.5 μm and 8.0 μm filters.

Model	χ^2_{min}	Age / Myr	E(B-V)	Mass / $10^{10} M_{\odot}$	Current SFR / $M_{\odot}\,\mathrm{yr}^{-1}$	b / $10^{-10}\mathrm{yr}^{-1}$
burst (SSP)	2.83	90.5	0.00	1.35	$0.00^{\dagger}$	0.00
$\tau = 10$ Myr	2.81	102	0.00	1.34	$0.05^{\dagger}$	0.04
$\tau = 30$ Myr	2.34	143	0.02	1.63	4.59	2.82
$\tau = 70$ Myr	1.61	255	0.00	2.05	7.88	3.84
$\tau = 100$ Myr	1.38	321	0.00	2.33	9.80	4.20
$\tau = 300$ Myr	0.94	641	0.00	3.41	15.2	4.47
$\tau = 500$ Myr	0.90	$905^{\diamond}$	0.00	4.35	17.0	3.92
$\tau = 1000$ Myr	0.97	$1280^{\diamond}$	0.00	5.46	21.1	3.86
continuous	1.15	$5000^{\diamond}$	0.00	7.93	15.9	2.00

† Ruled out because SFR below lower limit set by Lyman-α emission.

$^{\diamond}$ Ruled out as age is close to or exceeds 1 Gyr, age of Universe at $z \approx 6$

Table 3. Favoured model parameters of various SED fits for SBM03#1, metallicity = $Z_{\odot}$

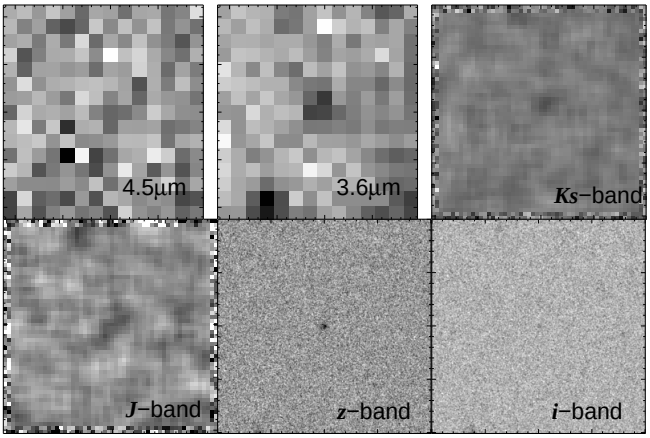

Figure 3. Images of GLARE#3001 ($z = 5.79$), taken with *HST*/ACS (i'- and z'-band); VLT/ISAAC J- and K_s-bands and *Spitzer* channels 3.6 & 4.5 μm. Each panel is 8 arcsec across (a projected distance of 50 kpc). The J and K_s band images have been smoothed using a 5-pixel box.

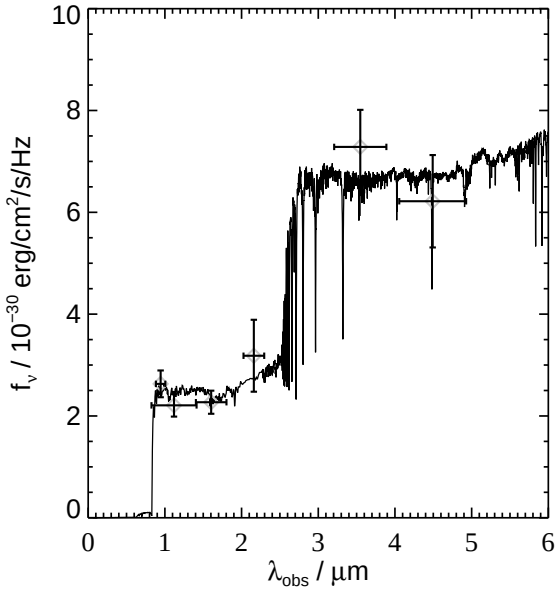

Figure 4. Best-fit Bruzual & Charlot model for SBM03#1: an exponentially decaying star formation rate with $\tau = 100$ Myr, viewed 320 Myr after the onset of star formation. The stellar mass is $2.3 \times 10^{10}\ M_{\odot}$. Flux density is in f_{ν} units.

3.1 Balmer/4000 Å Breaks in $z \approx 6$ Galaxies

The presence of a Balmer/4000 Å break is suggestive of a system viewed a significant time after a major epoch of star formation – the Balmer break at 3648 Å is strongest in an A-star population, and metal line blanketting (predominantly Fe II) due to an older late-type stellar population produces the 4000 Å break. For the two i'-drops with the best *Spitzer* detections (SBM03#1 & #3) we find evidence of a significant Balmer/4000 Å break: the brightening by a factor of 2 in f_{ν} from the near-IR ($\approx 0.9 - 2.2\,\mu$m) to 3.6 μm implies a break amplitude of $D4000 \approx 1.7$ (using the definition in Bruzual (1983) for f_{λ} flux densities). The z', J & K_s colours are relatively flat in f_{ν} (Figures 4 & 5) –ignoring the discrepantly faint K_s magnitude of SBM03#3– which favours the spectral break interpretation rather than dust reddening (see Section 3.5).

For all the galaxies discussed here, there has been recent or ongoing formation of at least *some* massive stars prior to the epoch of observation, as our Keck/Gemini spectra show Lyman-α emission produced through photoionization of hydrogen by the short-lived OB stars (Bunker et al. 2003; Stanway et al. 2004a). In order to produce the

Model	χ^2_{min}	Age / Myr	E(B-V)	Mass / $10^{10} M_\odot$	Current SFR / $M_\odot\,\mathrm{yr}^{-1}$	b / $10^{-10}\mathrm{yr}^{-1}$
burst (SSP)	1.54	114	0.00	1.32	0.00†	0.00
$\tau = 10$ Myr	1.50	128	0.00	1.35	0.02†	0.01
$\tau = 30$ Myr	1.30	161	0.01	1.42	2.23†	1.57
$\tau = 70$ Myr	0.99	255	0.00	1.59	6.12	3.84
$\tau = 100$ Myr	0.87	321	0.00	1.83	7.70	4.20
$\tau = 300$ Myr	0.77	641	0.00	2.77	12.4	4.47
$\tau = 500$ Myr	0.78	905$^\diamond$	0.00	3.57	14.0	3.92
$\tau = 1000$ Myr	0.81	1280$^\diamond$	0.00	4.54	17.5	3.86
continuous	0.93	2600$^\diamond$	0.02	4.34	16.7	3.85

† Ruled out because SFR below lower limit set by Lyman-α emission.
$^\diamond$ Ruled out as age is close to or exceeds 1 Gyr, age of Universe at $z \approx 6$

Table 4. Favoured model parameters of various SED fits for SBM03#1, metallicity = $0.2 Z_\odot$

Model	χ^2_{min}	Age / Myr	E(B-V)	Mass / $10^{10} M_\odot$	Current SFR / $M_\odot\,\mathrm{yr}^{-1}$	b / $10^{-10}\mathrm{yr}^{-1}$
burst	3.66	47.5	0.00	1.12	0.00†	0.00
$\tau = 10$ Myr	3.65	64.1	0.00	1.17	1.93†	1.64
$\tau = 30$ Myr	3.21	114	0.00	1.53	11.7	7.64
$\tau = 70$ Myr	2.75	203	0.00	2.22	18.6	8.39
$\tau = 100$ Myr	2.55	255	0.00	2.54	21.5	8.48
$\tau = 300$ Myr	2.06	453	0.00	3.54	33.4	9.43
$\tau = 500$ Myr	1.96	641	0.00	4.78	36.8	7.69
$\tau = 1000$ Myr	1.88	905$^\diamond$	0.00	6.81	46.3	6.80
continuous	1.82	1800$^\diamond$	0.00	5.20	28.9	5.56

† Ruled out because SFR below lower limit set by Lyman-α emission.
$^\diamond$ Ruled out as age is close to or exceeds 1 Gyr, age of Universe at $z \approx 6$

Table 5. Favoured model parameters of various SED fits for SBM03#3, metallicity = $Z_\odot$

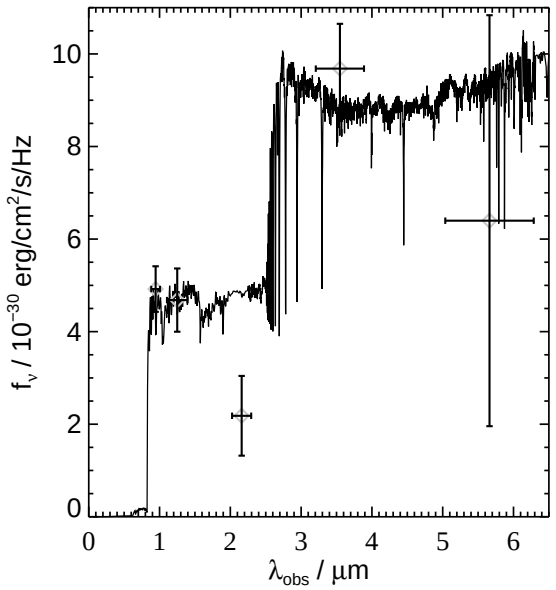

Figure 5. Best-fit Bruzual & Charlot model for SBM03#3: an exponentially decaying star formation rate with $\tau = 500$ Myr, viewed 640 Myr after the onset of star formation, and with a stellar mass of $4.8 \times 10^{10}\,M_\odot$. Flux density is in f_ν units.

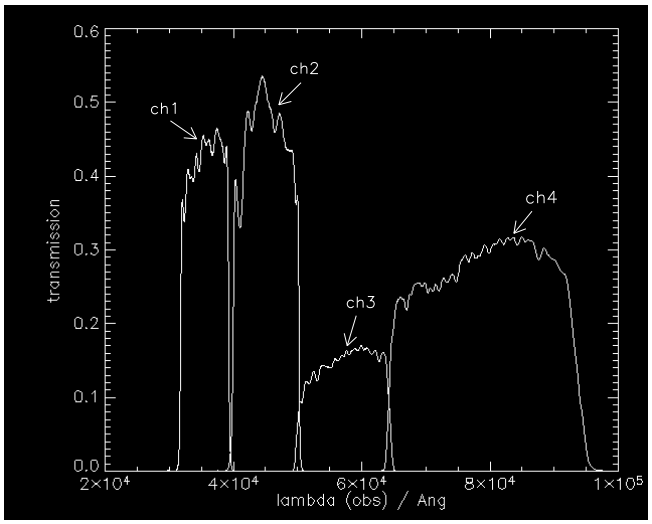

Figure 6. Filter profiles of the four *Spitzer* IR wavebands

Balmer break amplitude at $\lambda_{\mathrm{rest}} \approx 4000$ Å, most of the stellar mass probably formed well before the current starburst, most likely > 100 Myr previously (Section 3.2). Hence the galaxies SBM03#1 & #3 are already, to some extent, established. This is a significant finding since, at $z \approx 6$, the Universe is less than 1 Gyr old.

There is no significant evidence for a Balmer/4000 Å break in the two (fainter) spectroscopically-confirmed i'-drops: the $3\,\sigma$ detection of GLARE#3001 at 3.6 μm suggests a break of 0 ± 0.5 mag, and the non-detection of GLARE#3011 places a $3\,\sigma$ upper limit of $\Delta AB = 1$ mag on the break amplitude. Hence the constraints for the stellar ages of GLARE#3001 & 3011 are weak, but they are consistent with younger stellar populations than SBM03#1 & #3, which are brighter and presumably more massive. In the re-

Model	χ^2_{min}	Age / Myr	E(B-V)	Mass / $10^{10} M_\odot$	Current SFR / $M_\odot\,\mathrm{yr}^{-1}$	b / $10^{-10}\mathrm{yr}^{-1}$
burst	2.15	71.9	0.00	1.38	0.00†	0.00
$\tau = 10$ Myr	2.12	80.6	0.00	1.30	0.41†	0.32
$\tau = 30$ Myr	1.92	128	0.00	1.51	7.21	4.78
$\tau = 70$ Myr	1.73	203	0.00	1.81	15.2	8.38
$\tau = 100$ Myr	1.67	255	0.00	2.07	17.5	8.46
$\tau = 300$ Myr	1.50	453	0.00	2.96	27.9	9.42
$\tau = 500$ Myr	1.46	571	0.00	3.65	34.2	9.38
$\tau = 1000$ Myr	1.41	806$^\diamond$	0.00	5.37	43.3	8.07
continuous	1.36	1400$^\diamond$	0.00	4.34	25.1	6.97

† Ruled out because SFR below lower limit set by Lyman-α emission.
$^\diamond$ Ruled out as age is close to or exceeds 1 Gyr, age of Universe at $z \approx 6$

Table 6. Favoured model parameters of various SED fits for SBM03#3, metallicity $= 0.2 Z_\odot$

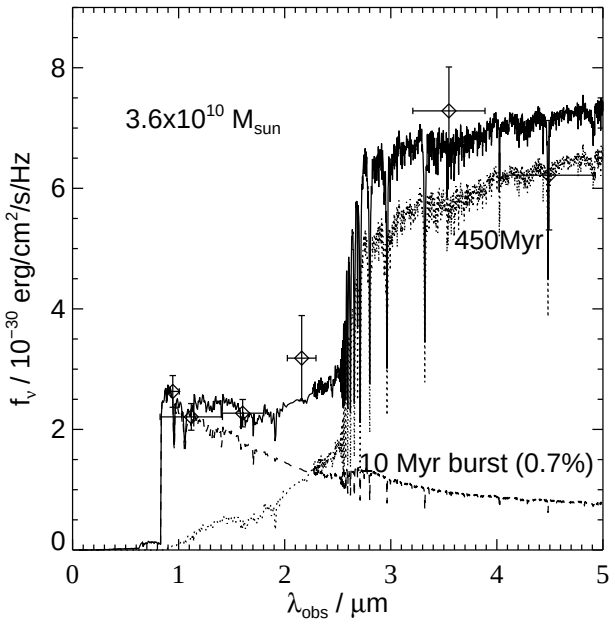

Figure 7. The best-fitting two-component stellar population model (Salpeter IMF) for SBM03#1: a dominant 450 Myr population of mass $3.6 \times 10^{10}\,M_\odot$, with some ongoing star formation activity (a burst for the last 10 Myr involving 0.7% of the stellar mass). Using a Chabrier IMF produces an identical best-fit age, with a similar mass fraction in the burst (0.6%), but a 30% lower total stellar mass ($2.5 \times 10^{10}\,M_\odot$.

mainder of this discussion, we focus on these two brighter sources, which have significant *Spitzer* detections for which we can estimate the stellar ages and masses.

3.2 Ages of the i'-drop galaxies

We explored the best-fit stellar ages and star formation histories of the galaxies SBM03#1 & #3 by comparing the SEDs from our broad-band photometry with the population synthesis models of Bruzual & Charlot (2003). We cover a range of star formation histories (presented in Tables 3, 4, 5, 6 & 7) designed to bracket most plausible evolution scenarios. Only a subset of these star formation histories provided acceptable fits to our photometry. We now discuss several classes of model and their validity.

We begin by considering an idealized "simple stellar population" (SSP) model, where a galaxy is viewed some time after its entire stellar mass formed in an instantaneous burst. These models provide relatively poor fits (reduced $\chi^2 \approx 3$ for solar metallicity) to our data. This is understandable given we know there is at least *some* ongoing star formation in both galaxies. The SSP models provide an absolute lower age limit for the bulk of the stellar mass. These SSP models yield an age of ≈ 100 Myr for the best fit population (and > 70 Myr at 99% confidence) in the absence of dust reddening (see Section 3.5), implying a formation redshift of $z_f \gg 6.4$.

At the other extreme, a constant star formation history was considered. The best fit ages in this simplistic scenario are 1.5-5 Gyr for metallicity $0.2-1\,Z_\odot$ (with SBM03#3 best-fit with a younger population than SBM03#1, and lower metallicities decreasing the age); these ages are obviously unphysical, as they exceed the age of the universe at this redshift (≈ 1 Gyr). This strongly implies that we are seeing both galaxies at an epoch when the star formation rate is declining, or that the current burst was preceded by a more significant episode of star formation.

Hence we next considered a range of more realistic models including an exponentially decaying star formation rate (SFR), such that the current $\mathrm{SFR}_t = \mathrm{SFR}_0\, e^{-t/\tau}$, where SFR_0 is the star formation rate at the onset of the burst and τ is the decay time in Myr. Such models are intermediate between SSP ($\tau \to 0$) and continuous star formation ($\tau \to \infty$) models. We considered several values of τ ranging between 10 Myr to 1 Gyr. As before, those models with ages older than the Universe at $z \approx 6$ were rejected. Also, models with $\tau = 10$ Myr were disregarded as they yielded current SFRs below the lower limit set by the Lyman-α emission (Section 3.6). The favoured models have an age of ≈ 600 Myr, with decay timescales of $\tau = 300$ Myr for SBM03#1, and $\tau = 500$ Myr for SBM03#3.

Finally, we consider a model where the galaxies are composed of two distinct stellar components: an ongoing starburst at the time of observation and an older population which formed in an instantaneous burst some time previously. We considered starbursts with a constant SFR which started 3, 10, 30, 100 & 300 Myr prior to the epoch of observation. We varied the ratio of total stellar masses in these two populations, and found the best-fit ages for the old component to be $400 - 500$ Myr. From the best-fit models (Table 7), the fraction of total stellar mass being formed in the starburst is $0.5 - 5\%$ for starbursts of $3 - 100$ Myr duration.

In summary, our SED fitting shows that the broad-band

burst duration	3 Myr	10 Myr	30 Myr	100 Myr
reduced χ^2	0.71	0.68	0.72	0.79
frac of mass	0.5%	0.7%	1.7%	5.2%
current SFR / $M_\odot\,\mathrm{yr}^{-1}$	60.0	25.3	19.0	68.3
age	400 Myr	450 Myr	450 Myr	450 Myr
stellar mass / $10^{10}\,M_\odot$	3.6	3.6	3.3	3.1

Table 7. Two-population composite models for SBM03#1, assuming an ongoing burst of constant star formation rate, commencing 3-100 Myr ago, within an older galaxy. The best-fit galaxy age and mass fraction of the starburst for each model are tabulated,

colours can be fit with a variety of stellar ages/star formation histories. The lower limit on the age is > 100 Myr (from an SSP model) with the oldest allowed models comparable to the age of the Universe at $z \approx 6$. Our best-fits to the broad-band photometry come from exponentially-decaying star formation histories, or a two-component model where only $0.5 - 5\%$ of the stellar mass is forming in an ongoing starburst. These best-fit models have mean stellar ages of $260 - 640$ Myr, which would require formation redshifts of $z_f \approx 7.5 - 13.5$.

3.3 Stellar Masses at $z \approx 6$

The SED fitting procedure described above leaves the normalisation of the Bruzual & Charlot model as a free parameter (along with the age for a particular input model). Our code outputs this normalization and, by using the luminosity distance to the i'-drop galaxies, we can calculate the corresponding best fit stellar mass for each star formation history. To assess the errors on the stellar mass estimates, we took the best-fit mass, $M_{\rm stellar}$, and recalculated the reduced χ^2 for the same age, metallicity and star formation history, but using total masses in the range $0.1 - 3\,M_{\rm stellar}$ (shown in Figure 8). In all our models, the stellar masses of SBM03#1 & 3 were $> 10^{10}\,M_\odot$ at 95% confidence ($2\,\sigma$). The lowest masses were returned by the SSP model, and the exponentially-decaying models with short decay times ($\tau \sim 10$ Myr): in fact, these models are unable to provide sufficient ongoing star formation to explain the lower limit set on the star formation rate by the Lyman-α emission (see Section 3.6). Our preferred models ($\tau = 70 - 300$ Myr and the two-component stellar population) have stellar masses of $\approx 2 - 4 \times 10^{10}\,M_\odot$ for a Salpeter IMF (we consider the impact of adopting a Chabrier IMF in Section 3.5).

We measure stellar masses from the best-fitting SEDs of $M > 2 \times 10^{10}\,M_\odot$ at $z \approx 6$. This is surprisingly large, supporting our contention that at least these two objects are well-established galaxies. The stellar mass is equivalent to 20% of that for a L^* galaxy today, using $L^*_r = -21.21$ from the SDSS analysis of Blanton et al. (2003) and taking $M/L_V \approx 5\,M_\odot/L_\odot$ (appropriate for a ≈ 10 Gyr old population from B&C models).

3.4 Stellar Mass Density and the Kormendy Relation

A key question given the increased information content on our two $z \approx 6$ sources is the likely descendant population and connection with systems seen at lower redshift. In this respect, we now consider the high surface brightness and small angular extent of the i'-drop galaxies.

To facilitate this discussion, we examine the properties of the $z \approx 6$ galaxies with reference to the $z \sim 0$ Kormendy relation between galaxy surface brightness and half-light radius (Kormendy 1977). Both SBM03#1 & #3 have half-light radii (effective radii) of $r_{hl} \approx 0\farcs08$ (Bunker et al. 2004; Bunker et al. 2003), and IRAC total magnitudes of $AB \approx 24$ at $3.6\,\mu$m (corresponding to the rest-frame V-band). The average surface brightness *within* the effective radius, $\langle I \rangle_{hl}$, is related to the average surface brightness *at* r_{hl}, I_{hl}, by $\langle I_{hl} \rangle = 3.6 \times \langle I \rangle_{hl}$ for a de Vaucouleurs profile (Ciotti & Bertin 1999). Hence our surface brightness at r_{hl} is $\mu_e = 21.6\,\mathrm{mag\,arcsec}^{-2}$.

Cosmological surface brightness dimming of $(1+z)^4$ will brighten this by -8.3 mag, and passive evolution from an age of ≈ 200 Myr at $z = 5.8$ to 12.8 Gyr at $z = 0$ would produce a luminosity dimming of a factor of $\times 30$ in V ($+3.7$ mag, using the B&C models). Hence, today we might expect SBM03#1 & #3 to have surface brightnesses of $\mu_e = 17.0\,\mathrm{mag\,arcsec}^{-2}$ for their half-light radii of $r_{hl} = 0.4$ kpc. In fact, the passively-evolved surface brightnesses sit comfortably on the present-day Kormendy relation (e.g., that of Ziegler et al. 1999 for cluster ellipticals), extrapolated to smaller scale lengths. Hence it seems that the inferred properties of these $z \approx 6$ galaxies are compatible with galaxy scaling relations at $z = 0$, subject to dimming through stellar evolution. Although our analysis has focused on only two of the most luminous systems, chosen by virtue of their luminosity, the possible implications are profound. What do these i'-drop galaxies at $z \approx 6$ evolve into? Given that these objects are barely resolved in the *HST*/ACS data with $r_{hl} < 0.5$ kpc, they are unlikely to passively evolve into the ellipticals today – which are typically larger. Merging would be required to explain the size evolution, although we note that the stellar masses and spatial scales of our $z \approx 6$ galaxies are similar to those of some spiral bulges today: a stellar age of ≈ 12 Gyr (Wyse, Gilmore & Franz 1997) today would imply a formation epoch of $z > 5$.

3.5 Effects of Metallicity, Dust and IMF on SED Fitting

When conducting the SED fitting, two metallicities were considered: solar ($Z_\odot$) and a sub-solar model ($0.2 Z_\odot$). The ages and masses of the best-fit models were similar for both metallicities, although the sub-solar model returned slightly better fits to the data, with smaller reduced χ^2_{min} values.

We also considered whether the red optical-IR colours (spanning the rest-frame UV to optical) could be attributable to dust reddening instead of, or as well as, an underlying old stellar population. To further examine this, we adopt the reddening model of Calzetti (1997)[6], appropri-

[6] The Calzetti reddening is an empirical law is given in terms of the colour excess $E(B-V) = 0.44\,E_{\rm gas}(B-V)$ with the wavelength dependence of the reddening expressed as:

$k(\lambda) = 2.656(-2.156 + 1.509/\lambda - 0.198/\lambda^2 + 0.011/\lambda^3) + 4.88$

for $0.12\,\mu\mathrm{m} \leq \lambda \leq 0.63\,\mu$m, and

$k(\lambda) = [(1.86 - 0.48/\lambda)/\lambda - 0.1]/\lambda + 1.73$

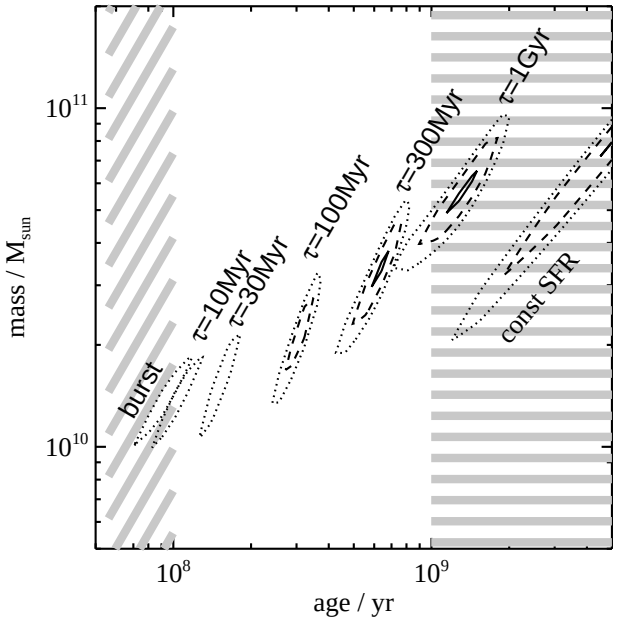

Figure 8. The allowed range of masses for several exponentially-decaying SFR models, with decay times ranging from $\tau = 10 - 1000$ Myr, as well as an instantaneous burst model and a constant SFR model. Those with stellar ages > 1 Gyr (right shaded region) are ruled out (the Universe is younger than this at $z \approx 6$. The models with ages $< 10^8$ yr are also excluded as they fail to produce the observed current SFR inferred from Lyman-α emission (left shaded region). Contours are 68% confidence (solid line), 95% confidence (dashed line) and 99% confidence (dotted line) for reduced χ^2 of $\approx 1, 2, 3$.

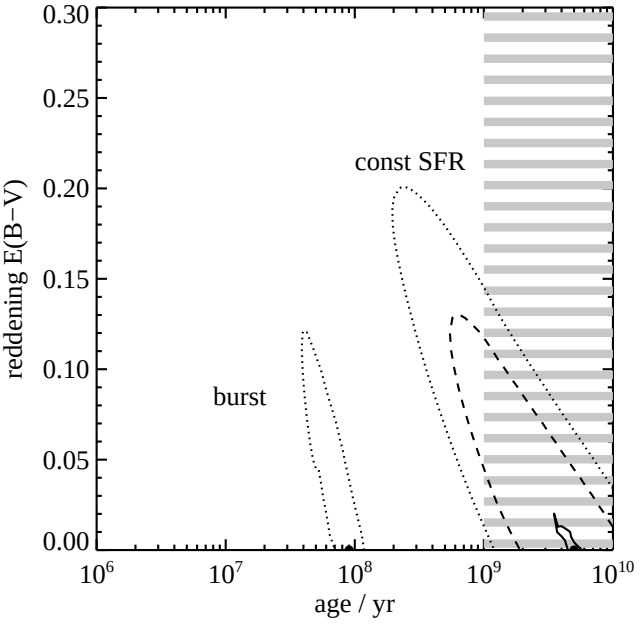

Figure 9. SBM03#1: A plot showing the reddening E(B-V) values for the two limiting scenarios of an instantaneous burst model and a constant SFR model, for the case metallicity $= Z_\odot$. Contours are 68% confidence (solid line), 95% confidence (dashed line) and 99% confidence (dotted line) for reduced χ^2 of $\approx 1, 2, 3$.

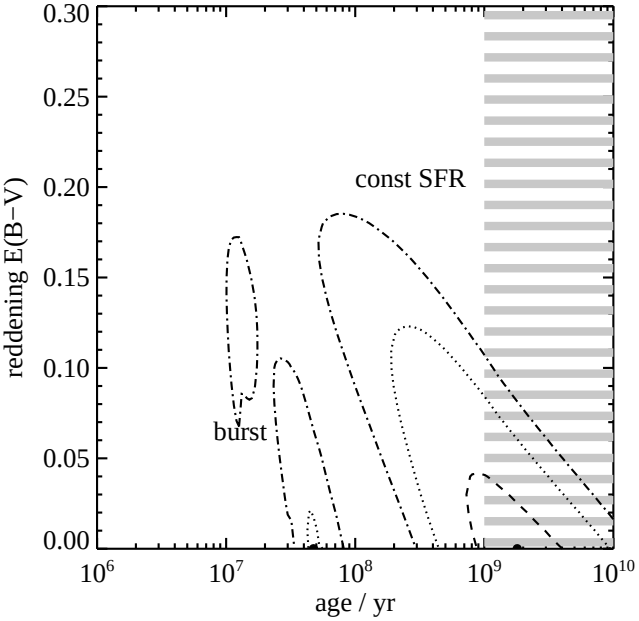

Figure 10. As figure 7, but for SBM03#3. Contours are for reduced χ^2 of $\approx 1, 2, 3, 4$, corresponding to 68% confidence (solid line), 95% confidence (dashed line), 99% confidence (dotted line), and $4\,\sigma$ confidence (dot-dash line).

ate to starburst galaxies. We constructed a grid of models for both the SSP (instantaneous burst) and constant SFR scenarios, using the Bruzual & Charlot templates over the full range of 221 age steps. For each age, we varied reddening in the range $E(B-V) = 0.00 - 1.00$ mag, in steps of 0.01 mag, computing the reduced χ^2 at each step. We find little evidence for substantial dust reddening in the detected starlight out to $\approx 5\,\mu$m: the formal best-fits for both SBM03#1 & #3 are no reddening. This is consistent with the flat spectral slopes in f_ν between the ACS z'-band and the NICMOS J- and H-bands reported by Stanway, McMahon & Bunker (2005) for many of the i'-drops in the *Hubble* Ultra Deep Field, including SBM03#1. The brightening in f_ν flux between the near-IR ($0.8 - 2.2\,\mu$m) and the IRAC bands at $3 - 5\,\mu$m is best explained by a spectral break rather than the smoother continuum gradient produced by dust reddening, and this is reflected in the best-fit stellar populations.

Finally, we tested the effects on the derived stellar masses of the assumed initial mass function. For the galaxy SBM03#1 (where the multi-waveband data was best, as it included NICMOS imaging in the near IR), we re-ran the 'two-population' model fits (Section 3.2) with a Chabrier (2003) IMF, instead of a Salpeter (1955) power law IMF. We used the same ongoing 10 Myr constant star formation rate burst, and fit for the age of an underlying older stellar population and the relative stellar masses of the burst and the old stars. Both IMFs produced comparably good fits (near-identical χ^2 values), the same 450 Myr

for $0.63\,\mu\text{m} \leq \lambda \leq 1.0\,\mu$m, and the flux attenuation is given by:

$$F_{\rm obs}(\lambda) = F_0(\lambda)\, 10^{-0.4E(B-V)k(\lambda)}$$

ages, and near-identical burst fractions (0.6% and 0.7% by mass for the Chabrier and Salpeter IMFs). The main difference came in the best-fitting total stellar mass: the Chabrier model produced a mass $\approx 30\%$ less than the Salpeter IMF ($2.5 \times 10^{10}\,M_{\odot}$ compared with $3.6 \times 10^{10}\,M_{\odot}$).

3.6 Star Formation Rates

We can usefully compare the ongoing star formation rate, the stellar mass and implied age, to deduce whether our two selected $z \approx 6$ galaxies are being seen during a fairly quiet or active period in their history.

First, let us consider the ongoing SFR. Star formation will dominate the rest-frame UV light (probed by the *HST*/ACS images) in the absence of dust obscuration or a significant AGN contribution. In our first analyses of i'-drop galaxies in the GOODS ACS images (Stanway, Bunker & McMahon 2003; Stanway et al. 2004a) and the Ultra Deep Field (Bunker et al. 2004), we used the conversion from rest-frame UV flux density to SFR, given by Madau, Pozzetti & Dickinson (1998), appropriate for continuous star formation. Based on the z'-band magnitudes we inferred unobscured SFRs of $19.5\,\&\,33.8\,M_{\odot}\,\mathrm{yr}^{-1}$ for SBM03#1 & #3, after accounting for Lyman forest blanketting of $D_A \approx 0.95$ shortward of Lyman-α.

The fits of the Bruzual & Charlot stellar synthesis models to the broad-band photometry provide estimates of the current SFR for a range of histories (Tables 3, 4 & 7). However, a firm lower limit arises from our Keck/DEIMOS spectroscopy (Bunker et al. 2003, Stanway et al. 2004a), which revealed Lyman-α emission. If this line emission is powered by ionizing photons from OB stars, then there must be star formation activity in these galaxies within the past 10 Myr (the lifetime of these stars, which dominate the Lyman continuum flux).

We have argued previously that the absence of X-ray emission and high-ionization lines such as N V 1240 Å, coupled with the narrow velocity width of the Lyman-α emission, renders an AGN interpretation unlikely. Our spectroscopy of SBM03#1 & #3 indicates line fluxes of $2 \times 10^{-17}\,\mathrm{erg\,s^{-1}\,cm^{-2}}$ for both sources, with rest-frame equivalent widths of $W_{\mathrm{rest}} = 30, 20$ Å. Assuming case B recombination and the same Salpeter IMF as in the Bruzual & Charlot models, the star formation rates from Lyman-α are $\approx 6\,M_{\odot}\,\mathrm{yr}^{-1}$. This may be treated as a firm *lower limit* on the current SFR, as the resonantly-scattered Lyman-α line is invariably quenched by dust to well below its case B line strength.

Our spectroscopic lower limit of an SFR $> 6\,M_{\odot}\,\mathrm{yr}^{-1}$ rules out the simple SSP model and those declining star formation rate models with the shortest decay rate ($\tau = 10-30$ Myr, Figure 8). Our favoured models are an exponentially decaying SFR with decay time $\tau \approx 300 - 500$ Myr, and two-component models with $1 - 2\%$ of the stellar mass created in an ongoing starburst of $10 - 100$ Myr. These all indicate similar SFRs to our original estimates of $\approx 20 - 30\,M_{\odot}\,\mathrm{yr}^{-1}$ from the z'-band flux.

Returning to the ratio of the current SFR to the stellar mass already formed, it is helpful to consider the '*b*-parameter' (e.g., Brinchmann et al. 2004) - a measure of the fraction of the total stellar mass currently being born as stars, defined as $b = \mathrm{SFR}/M_{\mathrm{stellar}}$. We measure $b \approx 4\,\&\,8 \times 10^{-10}\,\mathrm{yr}^{-1}$ for SBM03#1 & #3 (comparable with that inferred by Egami et al. (2005) from the *Spitzer* image a lensed galaxy with a photometric redshift of $z \approx 7$ (Kneib et al. 2004), and an indication of vigorous current star formation which supports the conclusion of this paper. However, the past-average SFR must actually be *greater* than the current SFR in order to build our $\approx 2 \times 10^{10}\,M_{\odot}$ galaxies, given the short time available prior to $z \approx 6$ (1 Gyr). This is why decaying SFR models appear to give the best fits to the SEDs.

Although our chosen galaxies are the brightest confirmed i'-drops in the GOODS-South field and possibly unrepresentative, the present work does support the inference that the low star formation density at $z \approx 6$ (Stanway, Bunker & McMahon 2003) compared to that necessary to reionize the Universe (Bunker et al. 2004) implies a yet earlier vigorous phase of activity. Indeed, the relative paucity of convincing $z \approx 7$ candidates and continuing low luminosity density at $z \approx 7$ seen in the NICMOS UDF (e.g. Bouwens et al. 2004) suggests that reionisation might have been achieved by a much higher star formation density at earlier epochs, consistent with the measurement of temperature-polarization correlation of the cosmic microwave background from the *Wilkinson MAP* satellite by Kogut et al. (2003).

4 CONCLUSIONS

Our group previously identified and spectroscopically-confirmed $z \approx 6$ galaxies through *HST*/ACS i'-drop imaging and Keck/DEIMOS & Gemini/GMOS spectroscopy. This paper presents the first IR detections of this population using *Spitzer*/IRAC. We have significant ($\approx 10\,\sigma$, $AB \approx 24$ mag) detections at $3.6\,\mu$m of the Stanway, Bunker & McMahon (2003) galaxies #1 and #3 (at $z_{\mathrm{spec}} = 5.83, 5.78$), and a more marginal detection of the $z_{\mathrm{spec}} = 5.79$ galaxy GLARE#3001 (Stanway et al. 2004b). We also detect SBM03#1 at $4.5\,\mu$m (SBM03#3 is outside the field of view of this $4.5\,\mu$m filter).

We infer from Lyman-α emission in our discovery spectra that there is ongoing star formation of $> 6\,M_{\odot}\,\mathrm{yr}^{-1}$ (as would be expected in these rest-UV-selected objects). However, the preceding star formation history has not been explored until now. In the two best-detected galaxies, we have evidence of a significant Balmer/4000 Å break, indicative of a prominent older stellar population which probably dominates the stellar mass. Exploring a range of population synthesis models indicates that the average stellar age is > 100 Myr; our best-fit models suggest preferred ages of $250 - 650$ Myr for an exponentially-declining star formation rate (of decay time $\tau \approx 70 - 500$ Myr) or a two-component model (with an ongoing starburst responsible for $0.5 - 5\%$ of the total stellar mass). This implies formation epochs of $z_f \approx 7.5 - 13.5$ for the galaxies SBM03#1 & #3.

In all our models, the best-fit stellar masses are $> 10^{10}\,M_{\odot}$, with 95% confidence masses of $2 - 4 \times 10^{10}\,M_{\odot}$. This indicates that at least some galaxies with stellar masses $> 20\%$ the mass of L^* galaxies today were already assembled within the first Gyr of the Universe. For these objects, the past average star formation rate is comparable to the current SFR, implying that there may have been even more

vigorous episodes of star formation at higher redshifts. These may have played a key role in reionizing the Universe, consistent with the earlier studies of Bunker et al. (2004) and Egami et al. (2005).

Acknowledgements

This work is based [in part] on observations made with the *Spitzer Space Telescope*, which is operated by the Jet Propulsion Laboratory, California Institute of Technology under NASA contract 1407. Observations have been carried out using the Very Large Telescope at the ESO Paranal Observatory under Program ID(s): LP168.A-0485. This paper is based in part on observations made with the NASA/ESA Hubble Space Telescope, obtained from the Data Archive at the Space Telescope Science Institute, which is operated by the Association of Universities for Research in Astronomy, Inc., under NASA contract NAS 5-26555. These observations are associated with proposals #9425 & 9583 (the GOODS public imaging survey). We are grateful to the GOODS team for making their reduced images public – a very useful resource. LPE acknowledges a Particle Physics and Astronomy Research Council (PPARC) studentship supporting this study.

REFERENCES

Becker R. H. et al., 2001, AJ, 122, 2850
Beckwith, S., Somerville, R., Stiavelli, M. 2003, STScI Newsletter vol 20 issue 04
Blanton, M.R., et al. 2003, ApJ, 592, 819
Bouwens, R.J., et al. 2004, ApJL, 616, 79
Brinchmann, J., et al. 2004, MNRAS, 351, 1151
Bruzual, G.A. 1983, ApJ, 273, 105
Bruzual, G.A., Charlot, S. 2003, MNRAS, 344, 1000
Bunker, A.J., et al. 2003, MNRAS, 342L, 47
Bunker, A.J., Stanway, E.R., Ellis, R.S., McMahon, R.G. 2004, MNRAS, 355, 374
Calzetti, D. 1997, AJ, 113, 162
Chabrier, G. 2003, PASP, 115, 763
Ciotti, L., Bertin, G. 1999, A&A, 352, 447
Dickinson, M.E., et al. 2004, ApJ, 600L, 99
Dickinson, M., Giavalisco, M. 2003, "Massive Galaxies at Low and High Redshift", p3224, ESO, Springer
Egami, E., et al. 2005, ApJL, 618, 5
Fazio, G.G., et al. 2004, ApJS, 154, 10
Ford, H.C., et al. 2003, SPIE, 4854, 81
Giavalisco, M. 2003, AAS, 202, 1703
Giavalisco, M., et al. 2004, ApJL, 600, 103
Giacconi, R., et al. 2002, ApJS, 139, 369
Kneib, J.-P., Ellis, R.S., Santos, M.R., Richard, J. 2004, ApJ, 607, 697
Kodaira, K., et al. 2003, PASJ, 55, L17
Kogut, A., et al. 2003, ApJS, 148, 161
Kormendy J. 1977, ApJ, 217, 406
Lacy, M., et al. 2005, submitted to ApJS
Madau, P., Pozzetti, L., Dickinson, M. 1998, ApJ, 498, 106
Oke, J.B., Gunn, J.E. 1983, ApJ, 266, 713
Reach, W.T., et al. 2004, "Infrared Array Camera Data Handbook version 1.0", Spitzer Science Center
Rhoads, J.E., et al. 2004, ApJ, 611, 59
Salpeter E. E., 1955, ApJ, 121, 161
Stanway, E.R., Bunker, A.J., McMahon, R.G. 2003, MNRAS, 342, 439
Stanway, E.R., McMahon, R.G., Bunker, A.J. 2005, MNRAS (submitted), `astro-ph/0403585`
Stanway, E.R., et al. 2004a, ApJ, 607, 704
Stanway, E.R., et al. 2004b, ApJL, 604, 13
Steidel, C.C., Pettini, M., Hamilton, D. 1995, AJ, 110, 2519
Steidel, C.C., Giavalisco, M., Pettini, M., Dickinson, M.E., Adelberger, K.L. 1996, ApJL, 462, 17
Steidel, C.C., Adelberger, K.L., Giavalisco, M., Dickinson, M.E., Pettini, M. 1999, ApJ, 519, 1
Stern, D., Spinrad, H. 1999, PASP, 111, 1475
Wyse, R.F.G., Gilmore, G., Franz, M. 1997, ARA&A, 35, 637
Yan, H., Windhorst, R.A. 2004, ApJL, 612, 93
Ziegler, B.L., Saglia, R.P., Bender, R., Belloni, P., Greggio, L., Seitz, S. 1999, A&A, 346, 13

This paper has been typeset from a TEX/ LATEX file prepared by the author.